

A critical assessment of theoretical methods for finding reaction pathways and transition states of surface processes

Jiří Klimeš¹, David R Bowler² and Angelos Michaelides¹

¹ London Centre for Nanotechnology and Department of Chemistry, University College London, London WC1E 6BT, UK

² London Centre for Nanotechnology and Department of Physics and Astronomy, University College London, London WC1E 6BT, UK

E-mail: angelos.michaelides@ucl.ac.uk

Received 9 July 2009

Published 3 February 2010

Online at stacks.iop.org/JPhysCM/22/074203

Abstract

The performance of a variety of techniques for locating transition states on potential energy surfaces is evaluated within the density functional theory framework. Diffusion of a water molecule across NaCl(001) and HCl bond breaking on the same surface are treated as general test cases; the former is an example of a low barrier diffusion process and the latter an example of a relatively high barrier covalent bond rupture event. The methods considered include the nudged elastic band (NEB), Dewar, Healy and Stewart (DHS), dimer, constrained optimization (CO), activation–relaxation technique (ART) and one-side growing string (OGS) as well as novel combinations of the DHS with growing string (DHS + GS) and DHS plus climbing image (CI-DHS). A key conclusion to come from this study is that the NEB method is relatively fast, especially when just a single (climbing) image is used. Indeed, using more images represents an unnecessary computational burden for our set of processes. The dimer method exhibits variable performance; being poor for the water diffusion processes, which have small activation energies, but much more efficient for the HCl bond breaking process which has a higher barrier. When only a poor initial guess of the transition state geometry is available, the CI-DHS scheme is one of the most efficient techniques considered. And as a means to quickly establish an approximate minimum energy pathway the DHS + GS scheme offers some potential.

(Some figures in this article are in colour only in the electronic version)

1. Introduction

Elementary processes at solid surfaces, such as molecular adsorption/desorption and diffusion, are of the utmost importance to a wide variety of disciplines including heterogeneous catalysis and the semiconductor industries. To be able to accurately determine the rates of these processes, which are often activated ‘rare’ events, is an important challenge to current computational materials modelling. Mainly this is because it requires not only determination of the initial and final state minima on the potential energy surface (PES) through which the reaction proceeds but also a determination of the relevant low energy transition state(s) (TS) that connect these local minima. Almost since the outset

of computational materials modelling, methods have been developed to efficiently determine such transition states and the minimum energy pathways (MEPs) that connect them to the initial and final states (see e.g. [1] or [2] for a review).

Here we test a selection of the methods popular in treating processes at surfaces using pathways where only one TS is present between the initial and final state. The methods considered include the nudged elastic band (NEB) [3–5], Dewar, Healy and Stewart (DHS) [6], dimer [7–9], constrained optimization (CO), activation–relaxation technique (ART) [10, 11] as well as novel one-side growing string (OGS) and combinations of the DHS with growing string (DHS + GS) and DHS plus climbing image (CI-DHS). We selected water diffusion on NaCl(001) and HCl

Table 1. Summary of the methods used in this study compared by the information they require, namely the need for a predefined final state geometry or guess of the reaction path or TS geometry. The ‘range for \mathbf{N} ’ gives the length scale that is used to approximate the direction of the minimal mode. Approximation by, for example, the vector between the initial and final states is labelled ‘global’. Information obtained from within ≤ 0.5 Å of the position of the image is labelled ‘local’. The NEB and DHS methods are described as ‘global–local’ because the former depends on the number of images used, and the latter becomes more local as the run progresses. We also show which methods are designed to converge to the TS geometry accurately. The methods listed are (CI-)NEB, climbing image-nudged elastic band; DHS(+GS), Dewar, Healy and Stewart (+growing string); CO, constrained optimization; ART, activation–relaxation technique; OGS, one-side growing string.

Method	Range for \mathbf{N}	Final state	Guess of pathway	Converges to TS	Reference
NEB	Global–local	Yes	Yes	No	[3]
CI-NEB	Global–local	Yes	Yes	Yes	[37]
DHS	Global–local	Yes	No	No	[6]
DHS + GS	Global–local	Yes	No	No	This work
CI-DHS	Local	Yes	No	Yes	This work
CO	Global	Optional	No	No	[38]
Dimer	Local	No	Optional	Yes	[7]
ART	Global	No	Optional	Yes	[39]
OGS	Local	Optional	No	No	This work

bond breaking on NaCl(001) as processes with which to test the various algorithms. These processes represent two distinctive classes of surface events: diffusion with a relatively low barrier (< 0.2 eV) and dissociation with a high barrier (> 1 eV). NaCl(001) is the lowest energy NaCl surface, the main exposed surface of salt crystals and as such plays an important role in atmospheric chemistry [12]. Water adsorption on this surface has been studied previously at various levels of theory [13–25] and experimentally [14, 26–32]. In this work we restrict ourselves to the low coverage water monomer regime. In contrast to the widely studied water/NaCl system, the interaction of HCl with NaCl has not received any attention.

Although studies comparing different TS search methods have been previously presented [1, 8, 33–35], many of them used empirical potentials for the evaluation of the energy and forces. Use of these potentials lacks one important feature of the *ab initio* calculations, namely the self-consistent field (SCF) procedure for determining the ground state electronic density. This iterative procedure has an impact on the calculation of the forces: while the forces are accurate and readily available using empirical potentials, in *ab initio* methods their accuracy depends on the convergence tolerance of the SCF procedure. A tighter convergence tolerance delivers more accurate forces but requires more computational time. Moreover, large changes in geometry between successive steps are no more costly than small changes with the empirical potentials but in the electronic structure calculations can require many more SCF iterations to update the electron density. Finally, for some especially poor initial guesses of the geometry the SCF procedure can even fail. Thus it is worthwhile to evaluate the performance of the various TS search methods directly within an electronic structure framework, which is what we do here.

In this study we evaluated the performance of a number of methods for locating TSs with density functional theory (DFT). Apart from several popular techniques we also developed three new algorithms: the ‘DHS + GS’ and ‘CI-DHS’ algorithms based on the DHS method, and a simple OGS technique. A key conclusion to come from this work is that the NEB method is relatively fast, especially when just a single (climbing) image is used. Indeed, for our set of processes, using NEB with

more images is an unnecessary computational expense. The performance of the dimer method depended strongly on the corrugation of the underlying PES: convergence towards the TSs was slow and problematic for the diffusion processes whereas it was fast for the dissociation reaction. The DHS + GS algorithm improves over the original DHS scheme and can be used to quickly establish an approximate MEP and TS. The guess of the TS can then be refined with the novel CI-DHS method. Overall, this scheme gives similar performance to the single image NEB in cases where the initial guess for the TS is poor, such as for HCl dissociation and some of the diffusion processes.

The remainder of the paper is organized as follows: the first part of section 2 gives short descriptions of the different methods. The second part of section 2 summarizes the computational set-up. Results for H₂O diffusion are provided in section 3 and for HCl bond rupture in section 4, with each method discussed separately. This is followed in section 5 with a brief discussion and conclusions.

2. Methods

2.1. Transition state algorithms

There are many methods for searching TSs and minimum energy pathways. Here we test several popular algorithms and combine some of them to produce new schemes. Specifically, the NEB, dimer, DHS, ART and CO methods are examined and two new techniques based on the DHS method, DHS + GS and CI-DHS, are presented. We also present an OGS method which is somewhat similar to the constrained optimization walk [36] and growing string methods [8].

In general, the various approaches considered here can be classified according to the amount of information they require in order to perform a search; specifically, if they require a predefined final state geometry or a guess of the TS. The particular requirements for the techniques tested are summarized in table 1. All methods considered here proceed by modifying the real force, \mathbf{F}_{real} , acting on the system by, for example, flipping the component of the force parallel to some direction \mathbf{N} :

$$\mathbf{F}_{\text{mod}} = \mathbf{F}_{\text{real}} - 2\mathbf{N}\mathbf{F}_{\text{real}} \cdot \mathbf{N}. \quad (1)$$

The modified force, \mathbf{F}_{mod} , then maximizes the energy along \mathbf{N} and minimizes it in all other directions. Therefore, when \mathbf{N} is aligned with the direction of the lowest frequency mode near to the TS, the force leads the system to the TS. The lowest frequency mode can, in principle, be obtained from the Hessian matrix. However, in practice the methods considered here approximate it in some way. A convenient approximation is to set \mathbf{N} equal to the vector between two states that lie at the bottom of the potential energy valley. In this case the more proximate the points are, the more accurately the minimal mode is obtained. We give the ranges of the length scales on the PES used for \mathbf{N} in table 1.

Let us now briefly describe the double-ended methods, namely NEB, DHS and CO. The NEB method (figure 1(a)) takes a set of images of the system between the initial and final states and optimizes them simultaneously in a subspace perpendicular to the imaginary line connecting the images. Additional forces keep the images evenly distributed along the pathway between the initial and final states. The TS can be located with the NEB method using the climbing image (CI) procedure, where the highest energy image is moved according to (1). When only a single image is used and allowed to climb (i.e. CI-NEB(1)) the method is equivalent to the force inversion method of Tateyama *et al* [10] with \mathbf{N} in (1) taken as a fixed vector between the initial and final states.

The DHS method uses two images starting from the initial and final states, with the lower energy image shifted towards the higher energy one in each step. Geometric optimization using only the component of the force perpendicular, \mathbf{F}_{\perp} , to the vector between the images is then performed. A few initial steps in this method are shown in figure 1(b), where it can be seen that the main idea is to bracket the TS from both sides. A typical problem with a DHS run is that it will fail if both images get on the same side of the TS during the optimization. To avoid this a smaller step must be used near the TS, which can lead to slow convergence towards the TS. Here we have improved the DHS method in two simple ways: first, we provide it with more information by using a sum of the regular DHS vector and a vector connecting the two previous images on the same side of the TS. This scheme which we dub ‘DHS + GS’ is schematically illustrated in figure 1(c). Second, we avoid the slow last stage of the DHS method near the TS and terminate the run when the distance of the two images drops below a predefined value. The last two frontier images and a third image made through their linear interpolation are then used as the initial, final and guess of the TS in a CI run from which the TS can be accurately identified. We call this scheme CI-DHS.

The CO method is one of the simplest approaches, and because of this it is widely used (see, e.g., [40]). In this approach some reaction coordinate (e.g. the distance between two atoms, the Cartesian coordinates of an individual atom) is chosen and the entire system is optimized subject to this constraint. After the forces converge a step is made along the reaction coordinate and a new optimization initiated. Here we start from the initial state and use the distance to the final state as the reaction coordinate. The optimization is then performed using only the forces perpendicular to the vector between the

current and final states. The CO procedure is well known to suffer hysteresis problems in some cases when approaching the TS from either the reactant or the product states (see, e.g., [1]).

The single-ended methods try to locate the TS without any reference to the final state. Usually they follow an energetic valley leading out of the energy minimum in the hope that a TS is located at the end of the valley. Some methods require the Hessian matrix, but this is unnecessary when only the minimal (softest) mode is to be followed. Methods from this class include the ‘dimer’, OGS techniques and ART. In the ART and the dimer methods the system follows \mathbf{F}_{mod} with different approximations of the minimal mode \mathbf{N} employed. For the ART we use a vector between the current geometry and geometry in a local minimum as \mathbf{N} . The initial geometry is taken as a structure close to the minimum geometry but displaced slightly along a predefined direction. The method then follows the force from (1) away from the minimum. The dimer method uses two images of the system with similar structures to find the minimal mode (figure 1(d)). The latter also calculates the curvature of the surface in the direction of the dimer and uses this as a switch in the modification of the force. When the curvature is positive, the system is driven only by the force parallel to the dimer, the full modified force is used in regions with negative curvature to find the TS. In the OGS method discrete steps are made towards the TS (figure 1(e)) which are followed by optimization using the component of the force perpendicular to the vector to the mean of the two previous images. The very first step in this procedure is obtained by displacing the initial geometry along a predefined direction and the initial guess for each subsequent point is taken as a linear extrapolation of the geometries of the two previous images.

We note one final point that is particularly relevant to the ART method, but also to the OGS and dimer techniques. Using just \mathbf{F}_{mod} means that *each* atom of the system is pushed away from its fixed reference. For the surface processes examined here, large moves of all surface atoms are not desirable. To avoid this a subset of atoms is defined and only the atoms in this subset are acted upon by \mathbf{F}_{mod} . This procedure is known as weighting and is equivalent to performing the search with a restricted set of reaction coordinates.

2.2. DFT computational set-up

The calculations were performed using the DFT plane-wave pseudopotential [41] approach, as implemented in the VASP code [42, 43]. The Perdew, Burke and Ernzerhof (PBE) [44] generalized gradient approximation (GGA) has been used throughout, along with projector augmented-wave (PAW) [45, 46] potentials. A 400 eV plane-wave cut-off has been used and the NaCl surface was modelled as a two-layer slab with the bottom layer held fixed. A Monkhorst-Pack \mathbf{k} -point mesh equivalent to $4 \times 4 \times 1$ per $c(1 \times 1)$ surface cell was used. This set-up was found to give water adsorption energies (E_{ads}) converged to within 15 meV of those obtained with a slab eight layers thick or an increased number of \mathbf{k} -points or a PW cut-off of 600 eV (table 2). The fact that this is such a benign system, converging rapidly

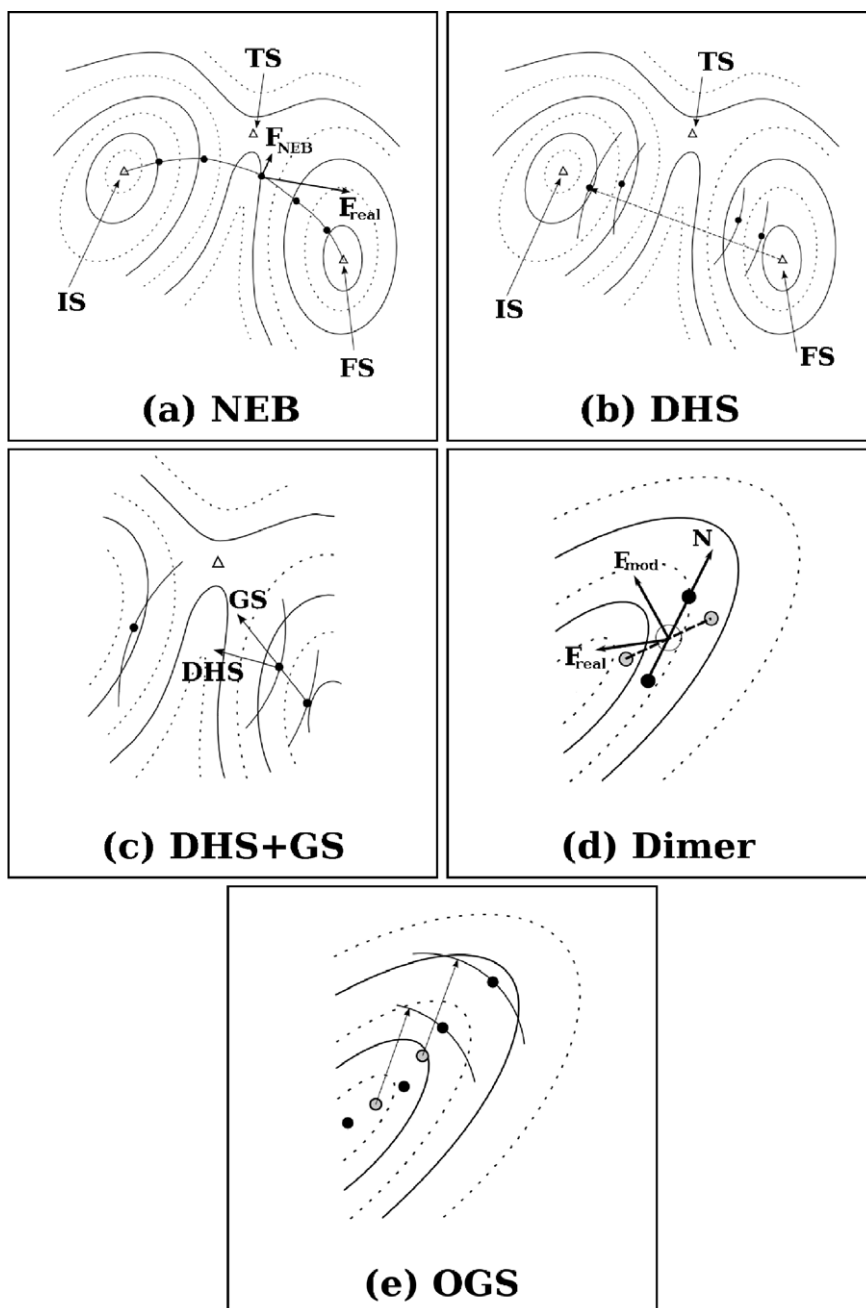


Figure 1. Schematic illustrations of some of the methods employed. (a) The NEB method is shown after a few steps with images connecting the initial and final states represented by black circles. The real force \mathbf{F}_{real} (shown for one image) is replaced by optimization of the force, \mathbf{F}_{NEB} , in a subspace perpendicular to the imaginary line that connects the images. (b) The DHS method tries to confine the TS from both sides using two images. During the procedure the image with lower energy makes a step towards the other image with subsequent constrained optimization. Here we show four initial steps. (c) In the DHS + GS method the step is not made directly towards the image on the other side of the TS (DHS arrow) but is combined with the vector connecting two previously converged images on the same side (GS arrow) in a defined ratio. (d) The dimer rotates (from grey circles to black circles) to find the direction that minimizes the sum of the energies of both images. The component of the real force \mathbf{F}_{real} that is parallel to the direction of the dimer \mathbf{N} is then inverted to produce a modified force, \mathbf{F}_{mod} , that is used in the geometry optimization procedure. (e) In the OGS method discrete steps are made followed by constrained optimization. Linear extrapolation of two previous images is used to supply a guess for the subsequent optimization which is performed with the distance constrained to the mean of two previous images.

with respect to the number of layers used, has been seen before [23, 47]. Aside from the convergence tests summarized in table 2, which were performed in a $c(1 \times 1)$ cell, a $c(2 \times 2)$ surface cell was used throughout, corresponding to a water coverage of 0.125 ML, where one monolayer (ML)

corresponds to one water molecule per surface NaCl pair. For this coverage the adsorption energy, E_{ads} , is -370 meV. This value is similar to those reported before using PBE and the PW91 exchange–correlation functionals [22–24]. However, it is less than the ~ -500 meV obtained recently by Li *et al*

Table 2. Adsorption energy of a water molecule on NaCl(001) for different number of layers in the slab. The adsorption energy, E_{ads} , is calculated according to: $E_{\text{ads}} = E_{m+\text{NaCl}} - (E_m + E_{\text{NaCl}})$, where $E_{m+\text{NaCl}}$ denotes the total DFT energy of the slab with the adsorbed molecule, and E_m , E_{NaCl} give the energy of a free molecule in the simulation cell and free slab, respectively. In each slab the bottom NaCl layer was held fixed and all other atoms allowed to relax. The tests reported here have been performed in a $c(1 \times 1)$ cell.

Number of layers	1	2	3	4	6	
E_{ads} (meV)	-359	-341	(-353) ^a	-343	-338	-345

^a Using a $6 \times 6 \times 1$ k -point mesh and a 600 eV plane-wave basis energy cut-off.

using accurate quantum chemistry methods and embedded cluster approaches [32]. This is probably due to an inaccurate treatment of long-range electron correlation in PBE.

A similar set-up was used for the calculation of HCl adsorption and dissociation. Additional convergence tests for this system established that the HCl adsorption energy and dissociation barrier were converged to within 10% of the values obtained on a four-layer slab. Since this process is examined merely as an example of one with a high barrier (~ 1.5 eV) this precision is sufficient for the present purposes.

The values obtained for the activation energies, E_a , are defined as

$$E_a = E_{\text{TS}} - E_{\text{IS}}, \quad (2)$$

where E_{TS} and E_{IS} are the adsorption energies of the TS and initial states, respectively.

The TSs used for reference purposes have been converged with extremely accurate settings (forces < 0.001 eV \AA^{-1}) with either the CI-NEB or the dimer method and confirmed with vibrational frequency analysis. When the performance of the different TS search methods in identifying the reference TSs is compared a more practicable < 0.01 eV \AA^{-1} convergence tolerance is used. To aid comparison between the various methods we define the approximation of the TS for methods that do not converge to the reference TS as the point with the highest energy and \mathbf{F}_\perp converged to a given criterion (for DHS, OGS and CO) or, for ART, as the first geometry with the real force pointing in the same direction as \mathbf{N} . Approximate TS structures are compared by determining the Euclidean distance³ of the approximate TSs from the reference TSs. We find that distances up to 0.2 \AA give a good representation of the geometry of the TSs and errors of only a few meV in E_a , whereas distances of ~ 1 \AA give bad geometries and energies. The general approach adopted in this study is illustrated by figure 2. The evolution of the total energy is shown for one TS algorithm (ART). The final structure identified is indicated by the black diamond, which resides about 83 meV above and 0.88 \AA away from the reference TS (violet circle) which was previously identified with NEB and confirmed with vibrational analysis.

³ The difference between two structures A and B is determined from $\Delta_{\text{geom}} = \sqrt{\sum_i (x_i^A - x_i^B)^2}$, where the sum runs over all coordinates, x_i^A and x_i^B , in the structures A and B, respectively.

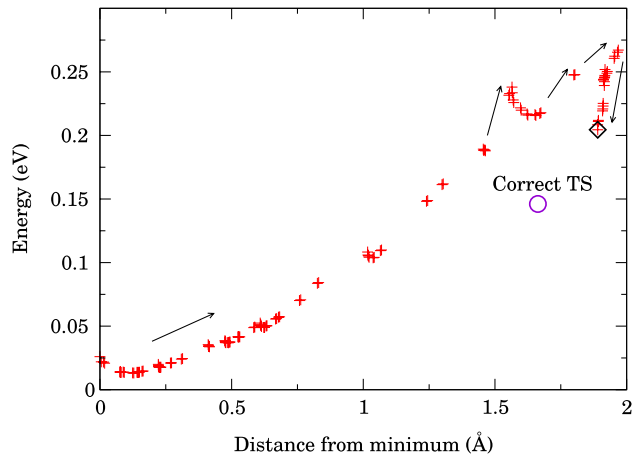


Figure 2. Energy versus distance from the minimum during an ART run towards the O-flip TS. The system follows a force inverted along the vector to the minimum and the progress of the method is illustrated by the arrows. The estimate of E_a is 228 meV after 120 steps (black diamond) compared to the NEB or dimer converged value of $E_a = 145$ meV (violet circle). Continuation of the run beyond 120 steps (not shown) did not lead to convergence to the correct TS.

The NEB method is implemented in VASP and some additional algorithms are available with the TSTools⁴ package. The other techniques tested or introduced here, which are not part of TSTools, have been implemented in a similar manner and are available on request. The TSTools package also contains force based optimizers that are suitable for use with the methods compared here.

3. Results for H₂O diffusion on NaCl(001)

The most stable geometry for water adsorption is shown in figure 3(a). The oxygen atom of the water molecule is located approximately above a Na^+ site, with the two OH bonds directed at adjacent Cl^- sites. This geometry is similar to the one observed in previous DFT calculations [22–24]. The location of the oxygen above the Na^+ matches the adsorption site suggested on the basis of helium scattering experiments for 1 ML coverage [14]. Due to symmetry there are four equivalent orientations of the water adsorption geometry from the perspective of Na^+ (and eight from the perspective of Cl^-). One can thus imagine many possible ways for water to move from one site on this surface to another. The question is which ones are relevant, i.e. what diffusion processes have low energy barriers. Three processes have been identified before by Cabrera-Sanfelix *et al* [23] and in this study a fourth has been determined⁵. We label the three previously identified processes according to [23] and call the newly found mechanism a ‘higher O-flip’. All the initial, transition and final states for the four processes are depicted in figures 3(b)–(e). Two of the processes involve only reorientation around the Na^+ adsorption site (OH-flip and parallel rotation) whereas

⁴ See: <http://theory.cm.utexas.edu/henkelman/code/>

⁵ We find here that one of the previously identified processes (H-flip) [23] goes through a stationary point with two imaginary frequencies.

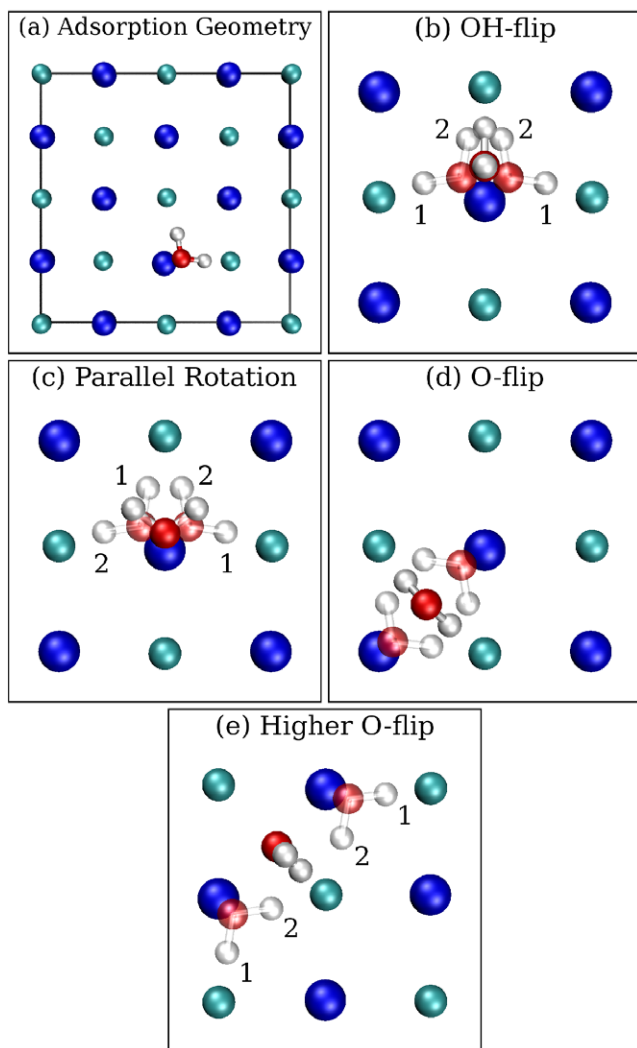


Figure 3. Equilibrium adsorption geometry (a) and four TS structures for water on NaCl(001). In (b)–(e) the initial and final states for each transition are shown in pale colours. The unit cell shown in (a) has been used for all studies, and only a small portion of it is shown in (b)–(e) for clarity. Similarly, labels have been added to the hydrogen atoms in the initial and final states. The initial guesses of the pathways for the NEB method go through geometries with the position of oxygen obtained by a linear interpolation of IS and FS structures and the hydrogen atoms added to form an H–O–H angle of 180° which makes such structures less biased. Na, Cl, O and H ions are represented by large blue, medium light green, medium red and small white spheres, respectively. This colour scheme is used throughout.

in the other two the water molecule moves from one Na^+ site to another (O-flip and higher O-flip). All processes involve molecular diffusion across a relatively static substrate. The E_a for each process is quite small: 50 meV for the OH-flip and 82 meV for the parallel rotation, in which the water molecule moves only around the Na^+ site; 145 meV for the O-flip and 166 meV for the higher O-flip, which lead to changes in the Na^+ adsorption site. Similar values were obtained by Cabrera-Sanfeliu *et al* [23] where the OH-flip, parallel rotation and O-flip processes were first identified and the small differences (22 meV for OH-flip, 9 meV for parallel rotation and 5 meV

for O-flip) can most likely be attributed to slightly different computational set-ups.

Using these established TSs, we then sought to see which methods could identify them or approximate them and how quickly this could be done. The main conclusion from these water diffusion studies, to be discussed in more detail below, is that the NEB method using a single climbing image was the most efficient algorithm at identifying the TSs. However, when only a poor guess of the TS geometry is available, the CI-DHS method introduced here was competitive. We now consider the results of each method separately, starting with those that require both initial and final state configurations.

3.1. NEB

The performance of the NEB approach in combination with the climbing image procedure is now discussed, dealing specifically with how the efficiency depends on the number of images⁶. The NEB method is known to be sensitive to the initial guess of the reaction pathway [8]. Here, in order to be as unbiased as possible the initial guesses of the pathways go through TSs that have been obtained through a linear interpolation of IS and FS structures, with the water molecule then adjusted to have a H–O–H angle of 180° . Overall, NEB proved to be robust and quite efficient at locating the TSs and mapping each MEP. Indeed, three out of four TSs were identified in a relatively small number of steps (<130 steps).

Assessing the effect of the number of images on the total performance, we give results for the NEB with one, three and eight images in table 3.⁷ All three set-ups converge to an identical TS and E_a . However, the main thing we find is that the total number of energy/force evaluations needed to converge the climbing image increases with the number of images used. Surprisingly, this also almost always involves a slight increase in the number of steps per image when more than one image is used. For example, for the OH-flip the number of steps needed to identify the TS increases from 127 to 579 to 1216 upon going from one to three to eight images. The increase in the number of steps per image arises because more images must be simultaneously converged to a certain value to let the climbing image converge to the TS. Of course, increasing the number of images is not entirely detrimental since more images generally improve the approximation of the full MEP. However, when only the TS structure and energy are of primary interest, using multiple images represents an unnecessary computational burden.

⁶ Tests with various geometric optimizers were also performed for a single image NEB run. These were largely in agreement with the results of [35]. Two of the TSTools optimizers (conjugate gradients (CG) and limited memory Broyden–Fletcher–Goldfarb–Shanno (L-BFGS) methods) converge in fewer steps (e.g. for the OH-flip CG needs 200 steps and L-BFGS 127 steps) than the default VASP optimizers (CG (278 steps) and modified Newton–Raphson scheme (>500 steps)) and than the other TSTools optimizers (fire, 493 steps).

⁷ A short NEB initial run with the QuickMin optimizer was performed and subsequent optimization using the climbing image used the global L-BFGS method (except for the three image parallel rotation run, where the CG method had to be used).

Table 3. Summary of the main results obtained for the four water diffusion processes considered, reporting the number of ionic steps (energy and force evaluations) needed to converge the geometry of the various TSs with a force accuracy of 0.01 eV \AA^{-1} or for the approximate methods (DHS, DHS + GS, ART, OGS, CO) to reach the highest energy point on the path. Also reported are the activation energies, E_a , in meV and the Euclidean distance, Δ_{geom} , in \AA of the approximate TSs from the reference TSs. The failure of a method to converge even approximately to a given TS is indicated by ‘F’. Diffusion processes not considered with a given method are indicated with a dash. Results for the DHS + GS method are shown for two levels of accuracy.

Method	OH-flip			Parallel rotation			O-flip			Higher O-flip		
	Steps	E_a	Δ_{geom}	Steps	E_a	Δ_{geom}	Steps	E_a	Δ_{geom}	Steps	E_a	Δ_{geom}
CI-NEB(1)	127	50		68	82		34	145		470	166	
CI-NEB(3)	579	50		210	83		132	145		—	—	—
CI-NEB(8)	1216	50		608	82		656	145		—	—	—
Dimer	F			F			337	145		600	166	
DHS ^a	272	90	0.67	126	112	0.71	147	146	0.14	375	196	0.66
DHS + GS ^a (H) ^b	250	80	0.66	111	109	0.67	136	149	0.23	249	180	0.44
DHS + GS ^a (M) ^b	255	74	0.58	88	108	0.70	105	140	0.19	333	178	0.46
CI-DHS ^a	302	50	0.04	179	82	0.08	155	145	0.02	433	166	0.06
ART	400	170	1.37	F			120	228	0.88	F		
OGS ^a	164	67	0.87	F			81	285	1.36	F		
CO ^a	251	107	1.00	62	150	0.81	73	181	0.53	291	280	1.00

^a A convergence criterion of 0.05 eV \AA^{-1} for perpendicular forces and a step size of 0.2 \AA were used.

^b Medium (high) settings in VASP correspond to an accuracy set to medium (high), the wavefunction convergence criterion 10^{-5} eV (10^{-6} eV), and the use of real (k -space) projectors. The computational cost is decreased by about a factor of three when medium compared to high accuracy settings are used.

3.2. DHS, DHS + GS, CI-DHS

In the DHS method two images of the system climb towards each other to meet at the TS. This technique performed reasonably well, approximately identifying all TSs. For the O-flip it performed particularly well, obtaining a TS within 1 meV of the reference one in 147 steps. However, the other activation energies are somewhat overestimated (up to 40 meV for the OH-flip) since the method does not always converge accurately to the precise TS structure. To improve the performance of DHS we developed two new algorithms: DHS + GS and CI-DHS.

In the DHS + GS algorithm more information about previous geometries is retained and used in order to improve the quality of the extrapolations made at each subsequent step. Specifically, as mentioned in section 2, we base the extrapolations on a sum of the regular DHS vector and a vector connecting the two previous images on the same side of the TS (see figure 1(c)). To test the influence of the GS-like step on the performance we ran several simulations for the OH-flip process with the DHS and GS contributions combined in proportions from 10:0 to 1:9. The optimal performance, which resulted in a 20% decrease in the number of steps was achieved for a 1:1 mixing ratio⁸. For all the other processes we therefore used a 1:1 mixing of the DHS and GS-like vectors which decreases the number of required steps by 10–30% and, with the exception of the O-flip, improves the final geometry.

In the CI-DHS method we combine the appealing features of the CI-NEB and the DHS methods: the ability of the DHS to confine the TS by walking from minima; and reliable

convergence to the transition state using two fixed images to approximate the transition mode. As shown in table 3, this combined method locates precisely the same TSs as the CI-NEB method. In the DHS part we found it expedient to use the DHS + GS variant just described and the CI procedure was started once the Euclidean distance of the frontier images was $<1 \text{ \AA}$. The total number of steps required is larger than that for the CI-NEB(1) method, with the exception of the higher O-flip where the CI-DHS performs the best out of all of the methods considered. In this case the CI-DHS needed 433 steps whereas CI-NEB(1) required 470 steps. The CI-DHS is superior to CI-NEB for this process because the method does not require a guess about the TS geometry—something which strongly influences the performance of the NEB method.

3.3. Constrained optimization (CO)

We now briefly discuss the CO technique in which the system makes steps from the initial to the final state with subsequent optimization in the direction perpendicular to the vector between the current and final states. Although this method, by construction, found pathways from the initial to the final states for each process, the overall performance was poor with the TS structures and energies identified differing significantly from the reference TSs. For all processes the errors in the geometry were in the range of $0.5\text{--}1.0 \text{ \AA}$ and the activation energies were off by as much as 114 meV. As for the DHS scheme the best result was obtained for the O-flip process with the TS error being 0.53 \AA and the barrier 36 meV higher than the accurate E_a . The poor performance of this method for water diffusion compared to, e.g., diffusion of a single atom across the surface or cleavage of a single covalent bond, where the CO method has been shown to offer adequate performance, is attributed to the greater complexity of the water diffusion PES. Specifically the processes examined here involve substantial rotations and

⁸ Increasing the GS part over this value leads to a decrease in performance because the images are more likely to end up in the same energy valley leading from the TS. We expect the 1:1 mixing to perform well in most situations, though there might be no improvement or even a decrease in performance compared to DHS for highly curved MEPs.

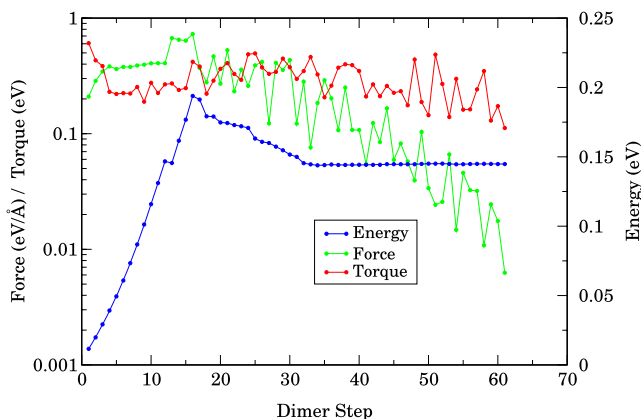


Figure 4. Energy (blue), force (green) and torque (red) acting on the dimer during the O-flip TS search. During the first part of the run, where the energy profile seems to be parabolic, the curvature is positive and the system only maximizes its energy along the minimal mode. When the curvature becomes negative, the system also minimizes energy in every other direction. The method converged to $0.01 \text{ eV } \text{\AA}^{-1}$ after 61 dimer steps (337 energy/force evaluations).

reorientations of the water molecule going through TSs that are poorly described by a linear interpolation of the initial and final states. For example, in the TS for the OH-flip the water molecule is upright (along the surface normal) whereas in the IS and FS the molecule is almost flat (parallel to the surface).

3.4. Dimer

Turning our attention to the single-ended approaches, we start with the dimer method. The dimer is a rather popular approach; however, for this particular system it exhibited variable or poor performance. When starting from the adsorption geometry, it failed to locate two of the four TSs: the OH-flip and parallel rotation. In addition, it only located the O-flip TS after a very large number of steps (337 compared to 34 with CI-NEB(1)) and with a ‘restrictive’ choice of parameters⁹. This particular search is shown in figure 4 where it can be seen that $\sim 50\%$ of the steps are spent on lowering the force from 0.1 to $0.01 \text{ eV } \text{\AA}^{-1}$ with energy already converged to within 1 meV . However, a very positive feature of the dimer method was that it was able to identify the higher O-flip TS, a TS that had not been identified before. Nonetheless this again required a very large number of steps (600), and, in general, for the water diffusion processes examined here the dimer method was thus rather inefficient.

In the original dimer paper [7] it was suggested that the dimer could be used as a scheme for refining the geometry of the TS from a preconverged NEB run with, for example, forces that are on the order of $0.1 \text{ eV } \text{\AA}^{-1}$. To this end we ran several dimer calculations starting from (CI-)NEB-preconverged geometries. These calculations converged for the O-flip and parallel rotation with default dimer parameters and for the OH-flip when a larger number (six) of rotations per step

⁹ The system converged only when the maximum step size was reduced to 0.1 \AA , more rotations were allowed (6) and a tighter torque criterion was set (0.5 eV).

and smaller geometry step (0.1 \AA) were used. However, we found that the dimer method was actually slower in converging to the TS for water diffusion than a simple continuation of the CI-NEB run. Although the real force is modified in the same way in both methods using equation (1), the mode \mathbf{N} is refined in each step in the dimer whereas in CI-NEB the \mathbf{N} is given by the geometries of the images adjacent to the CI.

3.5. ART

Moving to the simpler single-ended methods, we begin with the ART. Overall, this technique showed poor performance not converging to any of the TSs and only approximating the OH-flip and O-flip TSs with large errors in geometry and energy. The inversion of the force along the vector between the reference and actual geometries causes the force to point upwards towards the transition ridge independent of which side of the ridge the system is on. Therefore, when the system reaches the transition region, it simply hops back and forth. Figure 2 shows the energy versus distance from the minimum for an ART run directed towards the O-flip TS¹⁰. Although the method approximated this particular TS, continuation of the run did not lead to convergence with the estimate of the TS structure being 0.88 \AA away from the reference TS.

3.6. OGS

Finally, we discuss the performance of the OGS method, another new technique tested here. This approach was more successful than ART, decreasing the number of steps needed to approximate the TS and obtaining more accurate activation energies. However, as with ART, only two of the TSs were approximately located: the O-flip and the OH-flip TSs. Given that the other TSs (parallel rotation and higher O-flip) have higher activation energies and lie in a similar direction to the approximated TSs, we conclude that the ART and OGS methods preferably find lower lying transitions in a given direction. As an example of the OGS procedure, we show in figure 5 the evolution of the energy during two OGS runs directed towards the O-flip TS. The simulations are the same except for one when the weighting procedure is applied. Without weighting (red) the surface atoms tend to shift from their equilibrium positions which artificially increases the E_a . Weighting eliminates this problem, lowering the estimate of E_a for this process from 293 to 178 meV .

4. Results for HCl dissociation

So as to broaden the scope of this study and to evaluate the performance of some of the methods for a rather different surface process, in particular one with a considerably higher barrier, HCl bond breaking on NaCl(001) was examined. The initial and final states for this process, obtained through an extensive set of structure optimizations, are shown in figure 6. The initial state is a weakly adsorbed molecular state with an adsorption energy of -230 meV . In this structure the tilted HCl

¹⁰ The weighting procedure was used here so that only the force acting on the water molecule was modified.

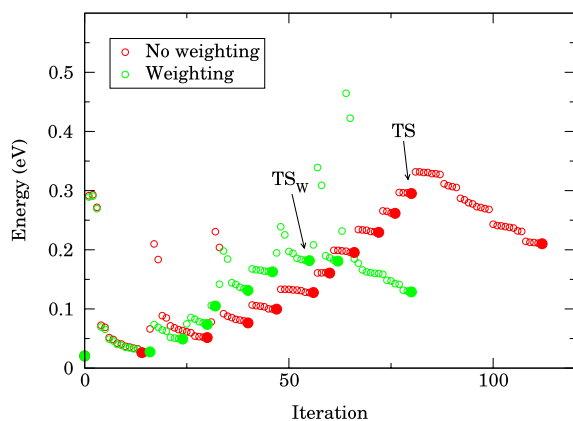


Figure 5. Energy versus number of ionic steps during two OGS runs from the energy minimum towards the O-flip TS (only parts of the runs are shown). In one run the weighting procedure (i.e. only the force acting on the water molecule is changed) was used (green) whereas in the other the modified force was applied to all atoms (red). The filled circles show the points at which the perpendicular forces F_{\perp} are converged with a convergence criterion of 0.05 eV \AA^{-1} . The estimate of E_a was 293 meV and 178 meV, after 80 and 55 steps, without and with weighting, respectively. The NEB or dimer converged value of E_a is 145 meV. The location of the transition state estimates without (TS) and with weighting (TS_w) are also indicated.

molecule rests along a surface Na^+Cl^- pair with the hydrogen end down. The final state is 1.45 eV higher in energy than the initial state and has the hydrogen inserted between two

surface Cl^- ions with a neighbouring Na^+ being considerably displaced upwards from its ideal lattice position. The pathway connecting these two states, obtained at first by NEB using eight images, is depicted in figure 7. With these initial and final states we then considered the efficiency with which the different methods identified the TS that separated them. The lowest energy TS identified for this process (figure 6) has an activation energy of 1.70 eV relative to the initial state, and the main results of the various methods tested are reported in table 4.

4.1. NEB

For HCl dissociation we again compare NEB with one, four and eight images between the initial and final states¹¹. In each case an equivalent TS was identified. However, we find again that extra images do not offer improved performance compared to a single image. Although the forces drop more smoothly for NEB runs with more images (figure 8), the single-image NEB run again converges in the fewest steps: 187 steps for one image compared to 432 and 1040 steps for four and eight images, respectively. Of course multiple images can also be

¹¹ To allow for a comparison of the methods, the same procedure was used with each number of images. First a linear interpolation was used to obtain the initial guess of the images and only after 25 steps was the climbing image procedure switched on. In addition, we note that a similar number of steps to converge was found for the CG and L-BFGS optimizers for four and eight images. However, the L-BFGS optimizer seems to require higher wavefunction accuracy (one order) and the CG optimizer performs better when the system starts further from the TS.

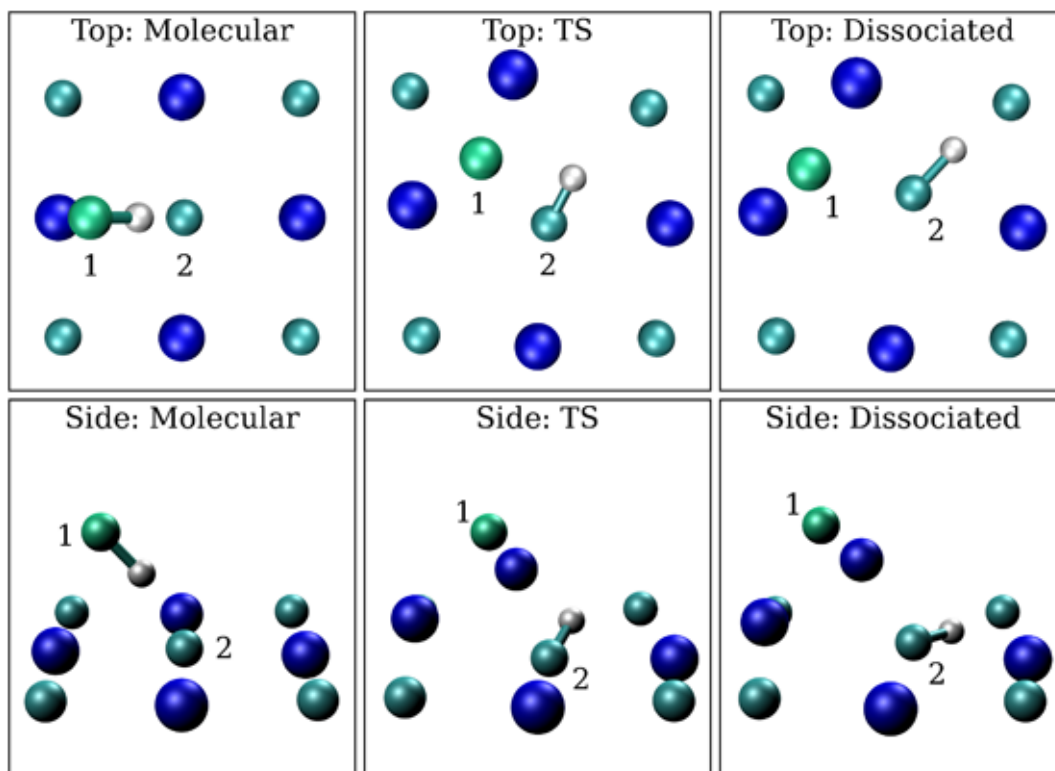


Figure 6. Top and side views of molecularly adsorbed (left), TS (middle) and dissociated (right) states for HCl on NaCl(001). The process involves the cleavage of the H–Cl(1) bond followed by the formation of the H–Cl(2) bond and the ejection of a Na from the lattice which then forms a new bond with Cl(1). Note that only part of the surface is shown.

Table 4. Number of ionic steps needed to converge to the TS for HCl dissociation at NaCl(001) with a force tolerance of $0.01 \text{ eV } \text{\AA}^{-1}$. The errors in the geometry and energy estimates compared to the dimer method with forces converged to $0.001 \text{ eV } \text{\AA}^{-1}$ are given. Two data sets for the DHS and DHS + GS methods refer to different accuracy settings with $\mathbf{F}_\perp = 0.05 \text{ eV } \text{\AA}^{-1}$ for ‘M’ and $\mathbf{F}_\perp = 0.01 \text{ eV } \text{\AA}^{-1}$ for ‘H’. The data for the CI-DHS method are divided into the DHS and CI parts of the calculation.

Method	CI-NEB(1)	CI-NEB(4)	CI-NEB(8)	Dimer	DHS (M/H) ^a	DHS + GS (M/H) ^a	CI-DHS
Number of steps	187	432	1040	192	188/262	182/228	121 + 52
Δ_{geom} (\AA)	0.15	0.16	0.12	0.06	0.62/0.62	0.63/0.63	0.45
ΔE_a (meV)	<1	<1	<1	<1	11/6	7/7	<1

^a Medium (high) settings in VASP correspond to an accuracy set to medium (high), wavefunction convergence criterion 10^{-5} eV (10^{-6} eV), and the use of real (k -space) projectors.

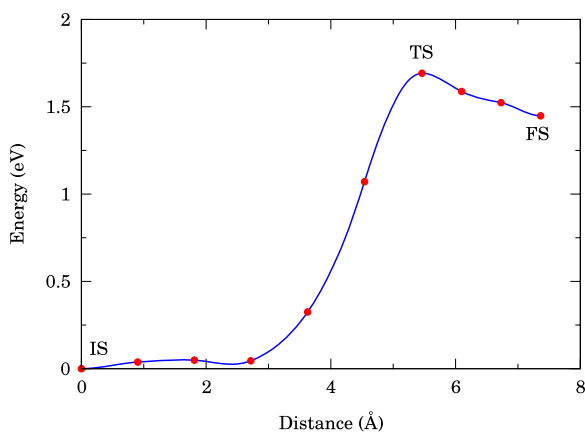


Figure 7. Energy pathway obtained for dissociation of HCl from an eight-image NEB run, with the climbing image converged to the TS. Each image is depicted by a red circle and the blue line was obtained by spline interpolation and should be regarded as a guide to the eye. The distance along the reaction coordinate was calculated by integration of the length along this spline.

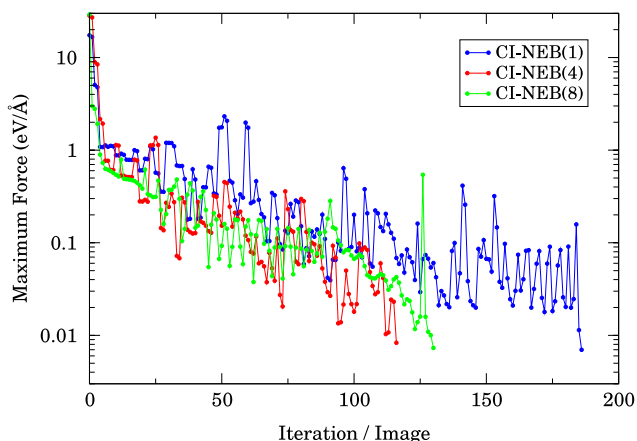


Figure 8. Maximum atomic force in the climbing image for one (blue), four (green) and eight (red) image NEB calculations for the HCl dissociation process. A conjugate gradient optimizer was used for the CI-NEB(1) and CI-NEB(4), whereas the global L-BFGS optimizer was used for CI-NEB(8).

used to obtain the full MEP rather than the TS alone (see figure 7). Nonetheless, if one is only interested in the height of the barrier using multiple images represents an unnecessary computational burden.

Table 5. Number of ionic steps needed to converge the DHS method for the HCl dissociation process and the resulting errors in energy and geometry for three values of \mathbf{F}_\perp at two different levels of accuracy.

Accuracy \mathbf{F}_\perp ($\text{eV } \text{\AA}^{-1}$)	High ^a			Medium ^a		
	0.05	0.02	0.01	0.05	0.02	0.01
Number of steps	145	204	262	188	294	431
ΔE_a (meV)	18	1	-6	11	6	-3
Δ_{geom} (\AA)	0.72	0.67	0.62	0.62	0.65	0.58

^a Medium (high) settings in VASP correspond to an accuracy set to medium (high), wavefunction convergence criterion 10^{-5} eV (10^{-6} eV), and the use of real (\mathbf{k} -space) projectors. The computational cost is decreased by about a factor of three when medium compared to high accuracy settings are used.

4.2. DHS, DHS + GS, CI-DHS

For this reaction the DHS algorithm was rather rapidly able to identify an approximate TS structure. Specifically the DHS method identified the TS after 145 steps with an error of 18 meV and Δ_{geom} of 0.72 \AA . We explored in detail how the quality of the \mathbf{F}_\perp determinations and convergence criteria impacted upon the results obtained with a series of calculations at different \mathbf{F}_\perp values (0.05, 0.02 and $0.01 \text{ eV } \text{\AA}^{-1}$) and convergence settings. However, as can be seen from table 5, reducing the value of \mathbf{F}_\perp does not have a significant impact on the quality of the TS estimate, whereas it does have a big impact on the number of steps required to reach convergence. For this process, it is therefore not worthwhile to reduce the \mathbf{F}_\perp convergence tolerance below $0.05 \text{ eV } \text{\AA}^{-1}$. The DHS + GS approach was also considered and exhibited similar performance to the original DHS scheme (table 4). As we found for water diffusion the CI-DHS method was superior to conventional DHS leading to convergence to a much better quality TS after 173 steps. As can be seen from figure 9, the energy profile is also well reproduced compared to the NEB data (figure 7). Although the error in the geometry is rather large ($\Delta_{\text{geom}} = 0.45 \text{ \AA}$), the quality of the TS can readily be improved by using a tighter force convergence criterion during the CI procedure. For example a $0.001 \text{ eV } \text{\AA}^{-1}$ convergence criterion leads to $\Delta_{\text{geom}} = 0.004 \text{ \AA}$ after about another 150 steps, i.e. essentially the reference TS is located.

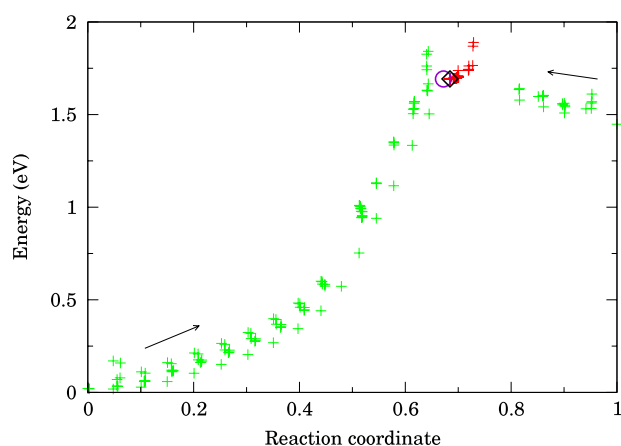


Figure 9. Energy versus reaction coordinate (distance from the initial state as a proportion of the total distance between the initial and final states) for the CI-DHS method for the HCl dissociation process. The DHS part is shown with green crosses with the two arrows indicating the progress of the two images. The subsequent climbing image part is shown in red. The TS identified is shown with a black diamond and the accurate (with a tighter convergence criterion) TS position with the violet circle.

4.3. Dimer

For HCl dissociation the dimer method performed much better than it did for H₂O diffusion. Indeed the number of ionic steps required to identify the TS was comparable to the CI-NEB(1) method. We note, however, that since the energy profile is asymmetric, the number of steps needed to reach the TS depends on whether the run starts from the initial or the final state. Whereas 192 ionic steps were needed to reach the TS from the final state, from the initial state 479 steps were required¹². Interestingly, although the dimer run that started from the final state needed slightly more ionic steps than the CI-NEB(1), each individual SCF optimization was completed in fewer steps and so less time overall was needed for the dimer to converge.

For the HCl dissociation reaction the dimer could also be used just to refine a guess about a TS obtained with one of the approximate methods. As a test of this approach we used the DHS + GS method to supply a suitable TS guess. The dimer run required a further 117 ionic steps to converge to the TS with a force tolerance of 0.01 eV Å⁻¹. Overall, this combination of DHS + GS followed by a dimer run required ~10% less computer time than a regular dimer run. Moreover, contrary to a single dimer run information about the whole pathway was obtained.

5. Discussion and conclusions

Let us now discuss in a broader context the performance of the various algorithms tested here. Overall, the NEB method with a single climbing image is superior to the other techniques when a suitable guess of the TS is available. Indeed for the processes examined here it was not necessary to use multiple

¹² The default set of parameters for the dimer was used in each case and the initial geometry was directed slightly towards the TS (by 0.15 Å).

NEB images. Of course using multiple images provides additional information about the shape of the MEP; however, if the TS alone is sought multiple images may be unnecessary. Nevertheless, in cases where interpolation between the IS and FS can be easily made, running a short NEB run with multiple images is a useful means to obtain a guess of the TS. The TS can then be refined using a CI-NEB(1) run with the highest energy image and the adjacent images used as the TS, IS and FS, respectively [4, 34]¹³.

In cases when only a poor initial guess of the TS is available and when both the initial and final states are known, then the modified DHS schemes presented here provide a means to approximate the MEP relatively quickly (DHS + GS) and to subsequently converge to the TS (CI-DHS). Indeed, in this cases the CI-DHS required fewer steps to converge to the TS than the CI-NEB(1) method. Moreover, the DHS method does not require as accurate forces as NEB (or dimer) and can therefore be used with lower accuracy settings that require less time to converge the SCF procedure. Overall the CI-DHS scheme offers some potential for further investigations given that it is a relatively simple technique, easy to implement and competitive with CI-NEB.

Performance of the ART and OGS methods was found to be unsatisfactory since both methods failed to identify the TS of the HCl bond breaking process and only some of the TSs were approximately identified for water diffusion. Selecting only some atoms to move according to the modified force (weighting) is essential for ART and improves the performance of the OGS method. However, application of the weighting procedure is less straightforward for processes that involve large displacements of the surface atoms, such as the HCl dissociation. The CO method had problems with reorientations of the water molecule which resulted in poor performance for water diffusion. The conclusion that the reaction coordinate driven methods (ART and CO) essentially fail for some processes is in agreement with previous studies [1].

The overall performance of the dimer method was rather poor for water diffusion. This is probably caused by the flat PES with several low energy modes of, for example, translation. On the other hand, we have some positive remarks: (i) a new TS was found with this method (the ‘higher O-flip’ process); (ii) unlike other methods the dimer did not correctly identify the ‘H-flip’ stationary point which has two imaginary frequencies with our set-up and was previously suggested to be a TS [23]. For HCl dissociation, the dimer could easily align with the bottom of the deep PES valley and its performance was better than that of the NEB with any number of images. Thus, a clear conclusion of this study is that the dimer method is considerably more efficient when the PES to be explored is highly corrugated.

Let us conclude with a few more comments about the effects that arise in the TS search because of the SCF procedure used to evaluate the DFT energy. With each SCF iteration

¹³ For example, in the HCl dissociation case we used the first part of the NEB(8) run with 25 steps to approximate the pathway and then the highest energy image and its neighbours to perform the CI-NEB(1) run. This second calculation needed 71 steps to converge, giving 271 steps in total and an error in the geometry of $\Delta_{\text{geom}} = 0.19$ Å.

the values of the energy and forces are (usually) improved until a predefined convergence criterion is achieved. Therefore methods that rely on accurate forces, such as the dimer, in general require more SCF iterations than methods that do not converge accurately to the TS, such as DHS or OGS. Specifically, since forces and energies in two proximate points are compared in the dimer method, it needs a more tightly converged wavefunction with ΔE between two successive SCF steps at least one order lower than is required by the NEB method. Similarly for structure optimizations, the accuracy of the forces required by the NEB method increases as the converged MEP and TS are approached. A computationally efficient scheme to account for this is therefore to use a relatively poor SCF convergence criterion in the initial stages of the TS search followed by more accurate settings as the quality of the MEP improves and the TS is approached. A final aspect of the SCF procedure that is relevant here is the quality of the trial structures used. The structure interpolation used in some methods can lead to initial structures with very distorted geometries. For example for the OH-flip process, interpolation of the initial and final states leads to an initial guess of the TS in which one of the OH bonds is only 0.3 Å long. First, ten geometry optimizations need twice as many SCF steps as optimization of a structure near the adsorption minimum. Even worse, linear interpolation for the higher O-flip process puts the hydrogen atoms in the same place and running SCF would be meaningless. Similarly, the efficiency of the NEB with multiple images is also reduced by the fact that in typical NEB implementations within the electronic structure framework all images of the system are optimized in parallel and must wait for the slowest image to converge the SCF procedure. Therefore, initial structures that are far from the initial and final states can take many more SCF steps to become converged. In each of these cases an algorithm such as the DHS method will not suffer from such deficiencies.

Acknowledgments

JK and AM are supported by the EURYI award scheme (see: www.esf.org/euryi) and the EPSRC. DRB is supported by the Royal Society. We are grateful to the London Centre for Nanotechnology and UCL Research Computing for providing computational resources. Also via our membership of the UK's HPC Materials Chemistry Consortium, which is funded by EPSRC (EP/F067496), this work made use of the facilities of HECToR, the UK's national high-performance computing service, which is provided by UoE HPCx Ltd at the University of Edinburgh, Cray Inc and NAG Ltd, and funded by the Office of Science and Technology through EPSRC's High End Computing Programme.

References

- [1] Henkelman G, Jóhannesson G and Jónsson H 2000 *Progress on Theoretical Chemistry and Physics* ed S Schwartz (New York: Kluwer Academic)
- [2] Schlegel H B 2003 *J. Comput. Chem.* **24** 1514

- [3] Mills G, Jónsson H and Schenter G K 1995 *Surf. Sci.* **324** 305
- [4] Henkelman G and Jónsson H 2000 *J. Chem. Phys.* **113** 9978
- [5] Trygubenko S A and Wales D J 2004 *J. Chem. Phys.* **120** 2082
- [6] Trygubenko S A and Wales D J 2004 *J. Chem. Phys.* **120** 7820
- [7] Dewar M J S, Healy E F and Stewart J J P 1984 *J. Chem. Soc. Faraday Trans. II* **80** 227
- [8] Henkelman G and Jónsson H 1999 *J. Chem. Phys.* **111** 7010
- [9] Peters B, Heyden A, Bell A T and Chakraborty A 2004 *J. Chem. Phys.* **120** 7877
- [10] Heyden A, Bell A T and Keil F J 2005 *J. Chem. Phys.* **123** 224101
- [11] Tateyama Y, Ogitsu T, Kusakabe K and Tsuneyuki S 1996 *Phys. Rev. B* **54** 14994
- [12] Barkema G T and Mousseau N 1996 *Phys. Rev. Lett.* **77** 4358
- [13] Finlayson-Pitts B J 2003 *Chem. Rev.* **103** 4801
- [14] Korol E N and Posudievsky O Y 1986 *Surf. Sci.* **169** 104
- [15] Wassermann B, Mirbt S, Reif J, Zink J C and Matthias E 1993 *J. Chem. Phys.* **98** 10049
- [16] Stefanovich E V and Truong T N 1996 *J. Chem. Phys.* **104** 2946
- [17] Jug K and Geudtner G 1997 *J. Mol. Catal. A* **119** 143
- [18] Taylor D P, Hess W P and McCarthy M I 1997 *J. Phys. Chem. B* **101** 7455
- [19] Allouche A 1998 *Surf. Sci.* **406** 279
- [20] Stöckelmann E and Hentschke R 1999 *J. Chem. Phys.* **110** 12097
- [21] Engkvist O and Stone A J 1999 *J. Chem. Phys.* **110** 12089
- [22] Meyer H, Entel P and Hafner J 2001 *Surf. Sci.* **488** 177
- [23] Park J M, Cho J H and Kim K S 2004 *Phys. Rev. B* **69** 233403
- [24] Cabrera-Sanfelix P, Arnau A, Darling G R and Sanchez-Portal D 2006 *J. Phys. Chem. B* **110** 24559
- [25] Yang Y, Meng S and Wang E G 2006 *Phys. Rev. B* **74** 245409
- [26] Cabrera-Sanfelix P, Arnau A, Darling G R and Sanchez-Portal D 2007 *J. Chem. Phys.* **126** 214707
- [27] Barraclough P B and Hall P G 1974 *Surf. Sci.* **46** 393
- [28] Fölsch S, Stock A and Henzler M 1992 *Surf. Sci.* **264** 65
- [29] Bruch L W, Glebov A, Toennies J P and Weiss H 1995 *J. Chem. Phys.* **103** 5109
- [30] Ewing G E and Peters S J 1997 *Surf. Rev. Lett.* **4** 757
- [31] Peters S J and Ewing G E 1997 *J. Phys. Chem. B* **101** 10880
- [32] Dai Q, Hu J and Salmeron M 1997 *J. Phys. Chem. B* **101** 1994
- [33] Li B, Michaelides A and Scheffler M 2008 *Surf. Sci.* **602** L135
- [34] Olsen R A, Kroes G J, Henkelman G, Arnaldsson A and Jónsson H 2004 *J. Chem. Phys.* **121** 9776
- [35] Koslover E F and Wales D J 2007 *J. Chem. Phys.* **127** 134102
- [36] Sheppard D, Terrell R and Henkelman G 2008 *J. Chem. Phys.* **128** 134106
- [37] Abashkin Y and Russo N 1994 *J. Chem. Phys.* **100** 4477
- [38] Henkelman G, Uberuaga B P and Jónsson H 2000 *J. Chem. Phys.* **113** 9901
- [39] Rothman M J and Lohr L L 1980 *Chem. Phys. Lett.* **70** 405
- [40] Barkema G T and Mousseau N 2001 *Comput. Mater. Sci.* **20** 285
- [41] Michaelides A and Hu P 2001 *J. Chem. Phys.* **115** 8570
- [42] Payne M C, Teter M P, Allan D C, Arias T A and Joannopoulos J D 1992 *Rev. Mod. Phys.* **64** 1045
- [43] Kresse G and Hafner J 1993 *Phys. Rev. B* **47** 558
- [44] Kresse G and Furthmüller J 1996 *Comp. Mater. Sci.* **6** 15
- [45] Perdew J P, Burke K and Ernzerhof M 1996 *Phys. Rev. Lett.* **77** 3865
- [46] Perdew J P, Burke K and Ernzerhof M 1997 *Phys. Rev. Lett.* **78** 1396
- [47] Blöchl P E 1994 *Phys. Rev. B* **50** 17953
- [48] Kresse G and Joubert D 1999 *Phys. Rev. B* **59** 1758
- [49] Li B, Michaelides A and Scheffler M 2007 *Phys. Rev. B* **76** 075401